Recent results & developments from the Apollo event-based counting camera

Benjamin Bammes[1,*]

[1] Direct Electron LP (San Diego, CA USA) [*] Corresponding author (bbammes@directelectron.com)

Three Dimensional Electron Microscopy Gordon Research Conference 2025

Ultra-fast event-based electron counting

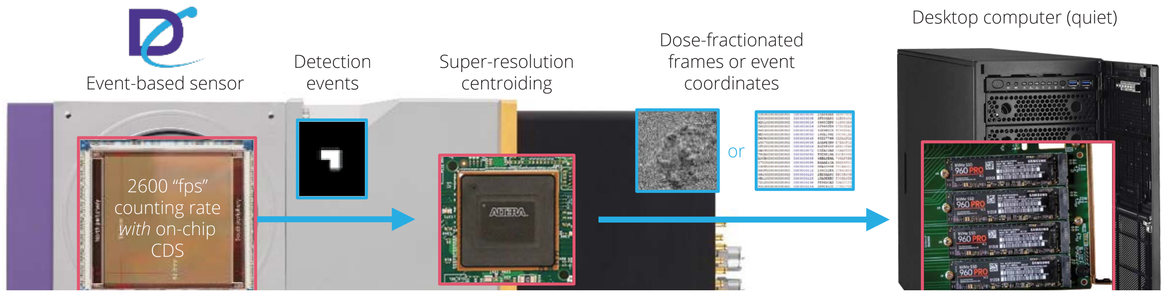

Figure 1: The Apollo is based on a novel (US Patent #10,616,521) ultra-fast, event-based, direct detection device (DDD®). Instead of outputting analog frames, the sensor detects incident electrons and outputs the location and shape of each detection "blob" registered on the sensor. On-chip correlated double sampling (CDS), on-chip thresholding, noise-free digital output, and ultra-fast counting speed maximize data quality.

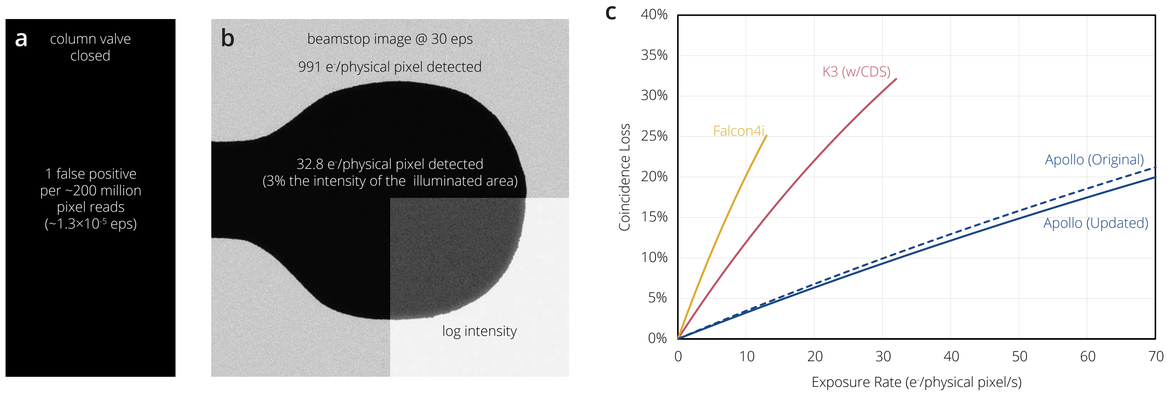

Figure 2: A recent firmware update has further improved the Apollo's performance. **(a)** A cropped region of a 4-second acquisition with the TEM column valve closed. The measured exposure over the entire sensor was ~1.3×10⁻⁵ e⁻/physical pixel/s (eps). **(b)** A cropped region of a 32-second acquisition of the TEM beamstop with an exposure rate of ~30 eps. Data acquired on a 200 kV TFS Glacios at Baylor College of Medicine. (Houston, TX). **(c)** The coincidence loss rate of the Apollo (from Peng, et al., 2022) compared to published data from other cryo-EM cameras (Nakane, et al., 2020 and Sun, et al., 2021). The "Apollo (Updated)" curve is scaled according to the increased counting speed in the recent firmware update.

Single-particle cryo-EM of feline calicivirus (FCV)

Charlotte Lewis, Lee Sherry, Joe Grove, Margaret Hosie, & David Bhella
MRC, University of Glasgow Centre for Virus Research (Glasgow, UK)

Cryo-EM of clinical isolates of FCV reveal a marked difference in capsid plasticity that correlates with virulence. In viruses associated with respiratory disease we find the capsid structure to be sharply resolved (**Fig. 3b & d**), whereas in strains associated with severe virulent systemic disease we find that the protruding capsid spikes (P-domains) are very flexible. Sharpened maps do not show density for this region (**Fig. 3e**), while unsharpened maps show low-resolution features (**Fig. 3f**). These data suggest that differences in capsid plasticity may be important in defining the virulence phenotype.

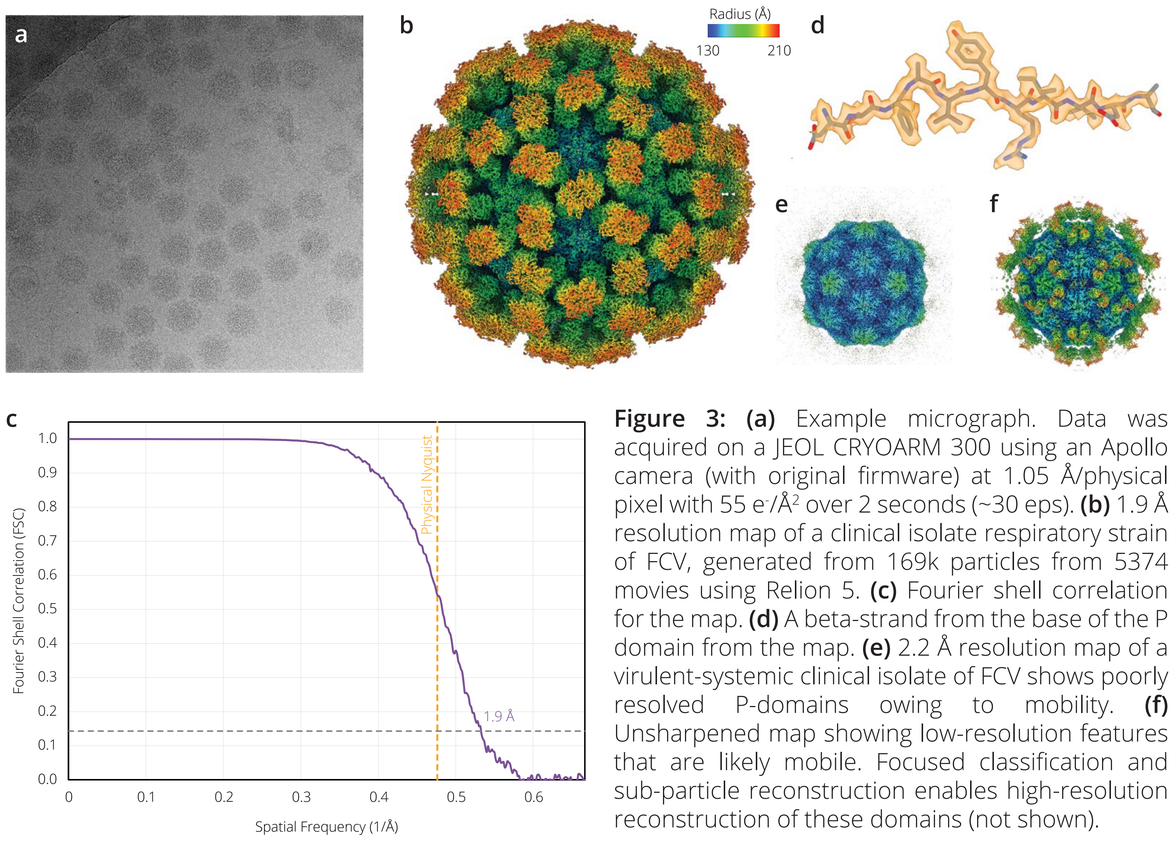

Figure 3: **(a)** Example micrograph. Data was acquired on a JEOL CRYOARM 300 using an Apollo camera (with original firmware) at 1.05 Å/physical pixel with 55 e⁻/Å² over 2 seconds (~30 eps). **(b)** 1.9 Å resolution map of a clinical isolate respiratory strain of FCV, generated from 169k particles from 5374 movies using Relion 5. **(c)** Fourier shell correlation for the map. **(d)** A beta-strand from the base of the P domain from the map. **(e)** 2.2 Å resolution map of a virulent-systemic clinical isolate of FCV shows poorly resolved P-domains owing to mobility. **(f)** Unsharpened map showing low-resolution features that are likely mobile. Focused classification and sub-particle reconstruction enables high-resolution reconstruction of these domains (not shown).

Optimizing magnification for single-particle cryo-EM

Figure 4: Estimated MTF of the Apollo camera at 300 kV (cyan) measured using a TEM beamstop (Peng, et al., 2022). The MTF is cropped at 1.5× Nyquist. The theoretical maximum MTF for a pixelated detector is shown in gray. For pixelated counting detectors with minimal backscattering, the shape of the MTF curve is monotonically decreasing. This poses a question: Is it better to acquire data at a high magnification so that the target resolution is closer to zero spatial frequency where the MTF (and the SNR) is higher?

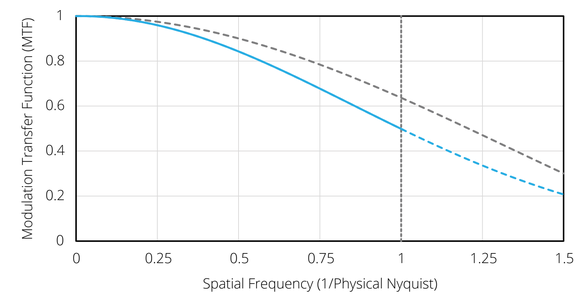

According to Rosenthal & Henderson (2003), the number of particle images (N_{part}) required to reach a resolution d for a 3D reconstruction of a particle with diameter D containing N_{asym} asymmetric units is given by:

$$N_{\mathrm{part}} = \frac{(\langle S\rangle^2/\langle N\rangle^2)\pi}{(\langle I_{\mathrm{obs}}\rangle/I_{\mathrm{o}})DN_{\mathrm{e}}N_{\mathrm{asym}}d}e^{-B_{\mathrm{overall}}/2d^2}$$

where $\langle S\rangle^2/\langle N\rangle^2$ is the required SNR for map interpretability, N_e is the exposure (typically in units of e⁻/Å²) that contributes to contrast (before radiation damage), $\langle I_{obs}\rangle/I_o$ is the average contribution to the structure factor SNR for each electron, and $B_{overall}$ is the "B-factor" describing the overall contrast loss of the experiment.

Here, we would like to disentangle some of the contrast loss effects caused by the detector and then use B_{other} to represent the contrast loss effects caused by all other factors.

The detection efficiency of a counting detector is defined by two factors: (1) the overall detective quantum efficiency (DQE) at zero spatial frequency (DQE_0) and (2) coincidence loss (Li, et al., 2013), which "down weights" the DQE at all spatial frequencies (Ruskin, et al., 2013). The fraction of detected electrons after coincidence loss (F_{det}) can be described according to the equation from Nakane, et al., (2020):

$$F_{\mathrm{det}} = \frac{1 - e^{-a\Phi_{\mathrm{pix}}}}{a\Phi_{\mathrm{pix}}}$$

where Φ_{pix} is the incident electron flux per physical pixel and a is the camera's coincidence loss constant. Then, the actual number of electrons that contribute to contrast generation at the target resolution is:

$$N_{\mathrm{e}}' = F_{\mathrm{det}}\mathrm{DQE}_0 N_{\mathrm{e}}$$

Additionally, the average contribution to the structure factor SNR for each detected electron, $\langle I_{obs}\rangle/I_o$, is reduced by the detector's attenuation of SNR, which is described by the detector's DQE:

$$\left(\frac{\langle I_{\mathrm{obs}}\rangle}{I_{\mathrm{o}}}\right)' = \left(\frac{\langle I_{\mathrm{obs}}\rangle}{I_{\mathrm{o}}}\right)\left(\frac{\mathrm{SNR_{out}}}{\mathrm{SNR_{in}}}(s)\right) = \left(\frac{\langle I_{\mathrm{obs}}\rangle}{I_{\mathrm{o}}}\right)\sqrt{\mathrm{DQE}(s)} = \left(\frac{\langle I_{\mathrm{obs}}\rangle}{I_{\mathrm{o}}}\right)\sqrt{F_{\mathrm{det}}\mathrm{DQE}_0}\mathrm{MTF}(s)$$

Therefore, accounting for the detector, the number of particles needed to attain the resolution of interest is:

$$N_{\mathrm{part}} = \frac{(\langle S\rangle^2/\langle N\rangle^2)\pi}{(\langle I_{\mathrm{obs}}\rangle/I_{\mathrm{o}})'DN_{\mathrm{e}}'N_{\mathrm{asym}}d}e^{-B_{\mathrm{other}}/2d^2} = \frac{1}{(F_{\mathrm{det}}\mathrm{DQE}_0)^{3/2}\mathrm{MTF}(S_{\mathrm{mag}})}\cdot\frac{(\langle S\rangle^2/\langle N\rangle^2)\pi}{(\langle I_{\mathrm{obs}}\rangle/I_{\mathrm{o}})DN_{\mathrm{e}}N_{\mathrm{asym}}d}e^{-B_{\mathrm{other}}/2d^2}$$

Let t be the exposure time, t_0 be the automation/camera overhead time per acquisition, S_{mag} be the fraction of Nyquist for the target resolution, N_{pix} be the number of pixels on the detector, and ρ_{part} be the particle density in the recorded images. Then the total acquisition time required (which we want to minimize) is:

$$T = N_{\mathrm{acq}}(t + t_{\mathrm{O}}) = \frac{4N_{\mathrm{part}}(t + t_{\mathrm{O}})}{{S_{\mathrm{mag}}}^2 d^2 \rho_{\mathrm{part}} N_{\mathrm{pix}}} = \frac{1}{{S_{\mathrm{mag}}}^2}\cdot\frac{t + t_{\mathrm{O}}}{(F_{\mathrm{det}}\mathrm{DQE}_0)^{3/2}\mathrm{MTF}(S_{\mathrm{mag}})N_{\mathrm{pix}}}\cdot\frac{4\pi(\langle S\rangle^2/\langle N\rangle^2)}{\rho_{\mathrm{part}}((I_{\mathrm{obs}}\rangle/I_{\mathrm{o}})DN_{\mathrm{e}}N_{\mathrm{asym}}d^3}e^{-B_{\mathrm{other}}/2d^2}$$

For a detector with good MTF and low coincidence loss, having more particles per image at lower magnifications has the greatest positive impact on total acquisition time. *We conclude that the optimal magnification for cryo-EM single particle experiments places the target resolution near physical Nyquist.*

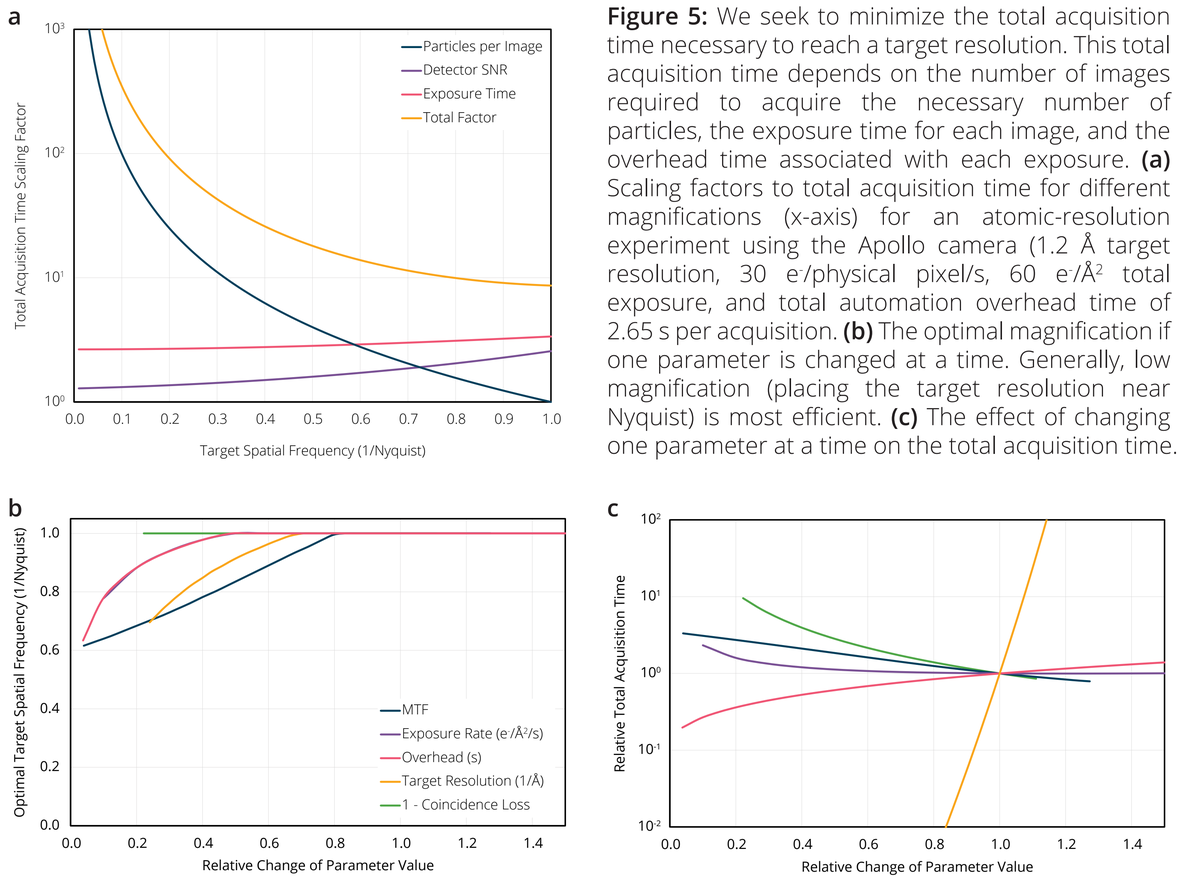

Figure 5: We seek to minimize the total acquisition time necessary to reach a target resolution. This total acquisition time depends on the number of images required to acquire the necessary number of particles, the exposure time for each image, and the overhead time associated with each exposure. **(a)** Scaling factors to total acquisition time for different magnifications (x-axis) for an atomic-resolution experiment using the Apollo camera (1.2 Å target resolution, 30 e⁻/physical pixel/s, 60 e⁻/Å² total exposure, and total automation overhead time of 2.65 s per acquisition. **(b)** The optimal magnification if one parameter is changed at a time. Generally, low magnification (placing the target resolution near Nyquist) is most efficient. **(c)** The effect of changing one parameter at a time on the total acquisition time.